Coherent Control of Light for Non-Line-of-Sight Imaging

Ilya Starshynov,* Omair Ghafur, James Fitches, and Daniele Faccio†
School of Physics & Astronomy, University of Glasgow, Glasgow G12 8QQ, United Kingdom

(Received 31 May 2019; revised manuscript received 26 September 2019; published 19 December 2019)

Non-line-of-sight (NLOS) imaging relies on collecting light that is rendered incoherent from multiple-scattering events and is then postprocessed to provide an estimate of the hidden scene. Here, we employ coherent phase control of the outgoing laser-beam phase front so as to refocus the beam behind the obscuring obstacle and then use the speckle memory effect to scan the focused spot across the scene. The back-reflected light intensity provides a direct measurement of the scene with a signal-to-noise ratio that is greatly improved when measured using a temporally gated detector. A spatial resolution of less than 1 mm is demonstrated, opening the way to high-resolution NLOS imaging.

DOI: 10.1103/PhysRevApplied.12.064045

I. INTRODUCTION

The imaging of objects that are not accessible to direct observation, also known as non-line-of-sight (NLOS) imaging, is a challenging problem with a variety of applications in biomedical imaging, autonomous robotics, defence, and security [1]. There exist a large number of proposed reconstruction techniques [2–10], which can be split into two major categories: those exploiting the time of flight (TOF) of the photons from the source to the hidden object [3,4,6,10] and those based on correlations of the intensity fluctuations of coherent scattered light encountering the object [2,7–9]. Although both of these categories require a diffusive scattering surface, the conditions of their applicability are different. The resolution of TOF methods is limited by the detector performance. The state-of-the-art single-photon-avalanche photodiodes (SPADs) offer a temporal resolution of 30 ps [11], which corresponds to a path difference of around 1 cm and, depending on the experiment geometry, allows the resolution of 1–10-cm features [5,6].

In the case of coherent light, diffusive scattering from a rough surface leads to random interference patterns called speckle, the intensity distribution of which can be controlled or even refocused by shaping the wave front of the incident field [12]. Moreover, the so-called speckle memory effect [13,14] implies that changing the incidence angle of the incoming wave causes the same tilt of the output speckle without changing its shape, assuming that the tilt is not too large.

Imaging methods based on this effect allow diffraction-limited reconstruction within the field of view, limited by the range of the memory effect (up to 1°). However, the information about the object shape is encoded into small variations of the raw data image intensity against a background that is proportional to the total object luminosity. This does not allow us to illuminate the object with the light diffusively scattered from the same rough surface due to the strong background signal, which also originates from the first reflection from the surface. Therefore, any of the speckle-memory-effect-based techniques known to us require a self-luminous object. In addition, the illuminated area on the rough surface increases when the object is moved away from it, which leads to smaller features in the raw data images and places constraints on the distance from the imaging sensor to the rough surface (10 cm in Ref. [9]).

Here, we combine memory-effect and TOF-based techniques to obtain high-resolution images of an object placed behind an occluding obstacle by coherent control of the light scattered from a rough reflective surface. We build a theoretical model that describes the main features of this configuration relevant to the choice of the experiment parameters, such as the angle of incidence and the optimal distance from the surface based on the physical parameters of the scattering medium. We use wave-front shaping to experimentally focus scattered light into a spot, which we are then able to scan within a particular region using the speckle memory effect. This allows us to achieve sub-millimeter spatial resolution, thus significantly improving TOF techniques.

II. REFOCUSING SCATTERED LIGHT FOR NLOS IMAGING

A. Description of setup

The setup is illustrated in Fig. 1. As a source of light, we use a Ti:sapphire pulsed laser (a Coherent Chameleon

*ilya.starshynov@glasgow.ac.uk
†daniele.faccio@glasgow.ac.uk

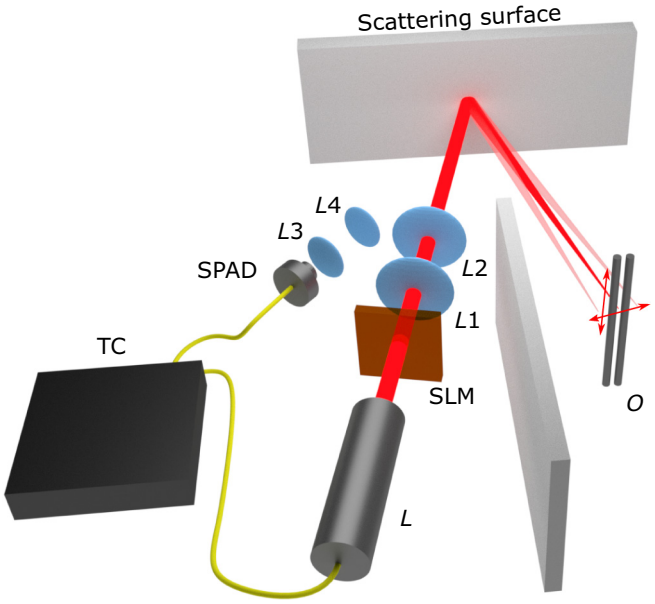

FIG. 1. The experimental setup. A pulsed laser (L) is shaped using a SLM, which is imaged onto a scattering surface. First, the SLM pattern is optimized to achieve a refocused spot in the scattered field and then an additional phase gradient is added to scan the spot. An image of the object, O, placed in the scanning region is reconstructed by measuring the intensity of the light reflected from the object and from the wall again. This light is separated from the background by acquiring TOF histograms of the scattered photons with a SPAD and a time-to-digital converter, TC.

Ultra) at the wavelength $\lambda = 810$ nm. The laser beam is expanded to fill the surface of a reflective spatial light modulator (SLM, Meadowlark 512×512 pixels, 7.68×7.68 mm active area), which is imaged onto a scattering surface (a brushed aluminum plate) with a demagnification factor of 0.8. In order to create a spot in the reflected speckle, we put a camera at the supposed position of the object and perform an optimization by measuring the reflection matrix of the surface. The light back scattered from the object when this is put in place of the camera is collected from a 3.5-cm spot on the scattering wall by means of a telescope focusing it to a SPAD. TOF histograms are collected at a 15 Hz repetition rate using a time-to-digital converter (TDC, ID900 IDQuantique) synchronized with the laser.

In most of the experiments reported in the literature related to scattered-light focusing, the incoming light is incident normally onto the scattering sample. However, since the speckle patterns become highly anisotropic at large scattering angles [15], in our experiment we tilt the incident wave front by approximately 6_10° with respect to the scattering surface. In order to maximize the memory-effect range, which depends on the light penetration depth to the scattering material, we use a rough (brushed) metallic surface as a scattering wall. This material retains some amount of specular reflection, which results in the increased directionality of the scattered light. This simplifies focusing and, more importantly, allows us to reduce the background return signal coming from the other objects in the scene.

B. Theoretical model

We wish to refocus the laser power into a spot at macroscopic distances, e.g., 10–100 cm from the scattering surface. The intensity enhancement of the refocused spot will be proportional to the number of modes at a given distance. We expect little enhancement very close to the surface, as speckle forms due to interference between various plane-wave components that occur only upon propagation away from the surface. On the other hand, in the limit of infinite distance, the speckle produced by the surface turns into a plane wave according to the Van Cittert–Zernike theorem [15], i.e., again, only one mode participates in the light intensity at any given point. At these two opposite regimes, no speckle refocusing (intensity enhancement) can be expected, which implies an optimal enhancement somewhere in between.

We first note that the angular spread of the reflected beam is described by [16]

$$\Omega(\psi,\theta,\phi) = \frac{[1-\cos(\theta)\cos(\phi)\cos(\psi)+\sin(\theta)\sin(\psi)]^2}{[\sin(\theta)+\sin(\psi)]^2} \exp\left(-\frac{\cos^2(\theta)+\cos^2(\psi)-2\cos(\theta)\cos(\phi)\cos(\psi)}{4s^2[\sin(\theta)+\sin(\psi)]^2}\right), \tag{1}$$

where $\Omega(\psi,\theta,\phi)$ is the relative amount of emission at the direction given by the inclination angle θ and azimuth angle ϕ, assuming that the rough surface is illuminated by a plane wave incident at an angle ψ, and s is the ratio between the average height and width of the surface-roughness features. Assuming that we illuminate a square area of a rough surface with a side L with a normally incident plane wave, the number of reflected modes directed at

a particular point in space is

$$N_\theta(x,y,z) = \frac{N_0}{L^2}\int\int_{-L/2}^{-L/2} \Omega\,(0,\theta(x+v,y+u,z),\\ \phi(x+v,y+u))\,dudv. \quad (2)$$

In the case of a rectangular illuminated area, the average width of the speckle grain changes with the distance from the surface as $\lambda z/L$, which leads to effective reduction of the number of modes with z at this rate. The resulting dependence of the number of modes on the distance from the surface d at a point (x_0,y_0) is therefore

$$N(d) = N_0 N_\theta(x_0,y_0,d)/L\lambda d. \quad (3)$$

Equation (3) has a maximum at a particular distance $d_{\max}$, indicating that, indeed, for a given scattering surface (described by s) and beam size, there is an optimal refocusing distance. We experimentally verify this by refocusing the laser spot (method described below) and measuring the dependence of the focused-spot enhancement on d [see Fig. 2(a)]. As can be seen, the maximum enhancement (which is specific for the surface that we use) is reached at a distance $d_{\max} \sim 40$ cm. In Fig. 2(a), we also show the fit of the theoretical dependence $N(d)$, Eq. (3), to our data, where the only fitting parameter is the normalization constant N_0, while s is determined by fitting N_θ, given in Eq. (2), which is proportional to the average intensity distribution of the scattered light, to an experimentally measured distribution [see Fig. 2(b)]. We perform all further experiments placing the object at this optimal distance of 40 cm. Figure 2(c) shows the experimentally measured depth of focus of the refocused spot, i.e., we fix the SLM phase pattern and then move the camera from 35 to 45 cm, hence measuring the focused-spot enhancement.

Figure 2(d) shows the full dependence of the optimal focusing distance $d_{\max}$ as a function of the surface parameter s and beam size. For a given diffusive surface, one can tune the optimal refocusing distance by changing the beam size; however, a small s or a large beam size also leads to a reduction in the actual peak-intensity enhancement: the solid black curve indicates the values for which the enhancement, with respect to the surrounding speckle, reduces to a factor of 100×, compared to 500× obtained for the surface that we use.

C. Optimization method

There exist a variety of optimization methods [17], ranging from the most simple continuous-sequential and partitioning algorithms [12,18] to more advanced genetic [19] or simulated annealing [20] algorithms. Alternatively, some methods exploit the physical properties of the scattering process; in particular, its linearity. The output modes are related to the input modes by means of a scattering

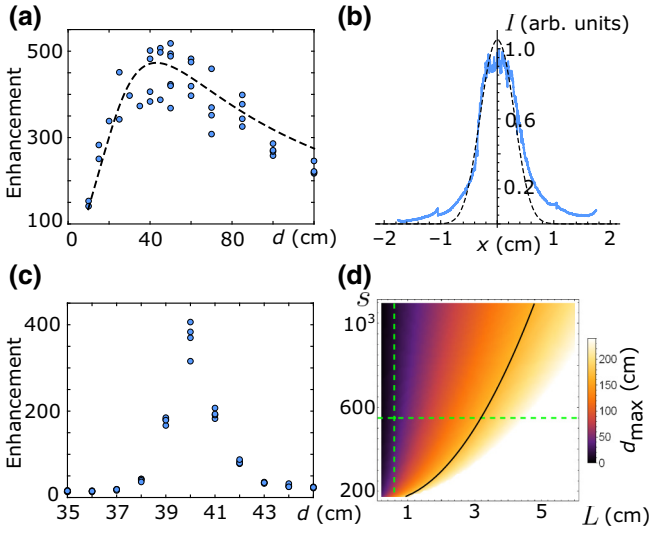

FIG. 2. (a) The dependence of the spot enhancement factor (the ratio of the focused spot intensity to the average background intensity) on the distance from the scattering surface, d, performing reoptimization of the SLM pattern at each distance. For each value of d, multiple measurements are performed, changing the illumination position on the surface. The dashed curve is a fit of $N(d)$ from Eq. (3) with the only fitting parameter $N_0 \approx 10^5$. (b) The average intensity of the reflected speckle at 40 cm from the scattering wall, from which we determine the directionality parameter $s \approx 550$ (dashed fitted curve). (c) The dependence of the spot enhancement on the distance from the scattering surface while keeping a fixed SLM pattern. (d) The dependence of the maximal enhancement distance $d_{\max}$ on the size of the illumination beam at the surface, L and s from Eq. (3). The green dashed lines denote the values used in our experiment and the black solid curve is a line of constant enhancement factor 100×.

matrix [21]. Knowledge of this matrix allows to design a configuration of the input modes required to achieve (almost) any desired output intensity distribution. Therefore, the optimization task reduces to measuring the scattering matrix of the disordered sample [22]. In practice, the major limiting factor defining the performance of any of these algorithms is the measurement noise [17]. In the case of bulk scattering media, the main source of speckle instability is sample alteration. As the speckle pattern is highly sensitive to the position of every single microscopic scatterer in the disordered material, it changes with temperature, humidity, and even ambient pressure for such samples [23]. In our case, the scattering-surface configuration remains stable over days and mechanical vibrations become the major source of instability. These deteriorate the performance of the algorithms that optimize the input pattern based on a single-output-spot intensity. The scattering-matrix measurement does not rely on a single output spot and is therefore less affected by the short-scale mechanical sample instability. For this reason, we use the scattering (reflection) matrix measurement to focus the scattered light in our experiment.

We measure the reflection matrix of the scattering surface using the internal reference method [24]. This method is a variation of a standard interferometric technique in which a set of phase patterns is selected and then each of them is shifted in four steps of $\pi/2$ with respect to a static reference while recording the resulting intensity distribution. In our case, the static reference originates simply from light reflected from the areas on the SLM not covered by the liquid-crystal pixels.

We use 64×64 Hadamard patterns as the basis and capture the intensity on a 100×100 pixel region of the camera for each of the $64 \times 64 \times 4$ measurements, from which the resulting reflection matrix is reconstructed. The input phase distribution leading to the focused spot in the output is then obtained as a product of the inverse of the measured matrix with the desired intensity image. We approximate the inverse of the reflection matrix by its Hermitian conjugate, effectively performing phase conjugation, since this method is more resilient to the measurement noise [24].

D. Scanning the focused spot

Knowledge of the scattering matrix allows us to get a focused spot at any of the 100×100 output positions. However, scanning the spot using the scattering matrix would make our method conceptually invasive, while the memory effect allows us to move the focus outside the region in which the scattering matrix is measured. Therefore, after we obtain a focused spot in the output speckle, we displace it by adding a linear phase gradient to the wave front incident on the SLM (see Fig. 3). In our experiment, we are able to shift the speckle spot by several millimeters [see Figs. 3(b) and 3(c)]. However, the main limiting factor is not the memory-effect range but, rather, the dimensions of the SLM. One full phase gradient from 0 to 2π across one of the dimensions of the SLM (7.68 mm) corresponds to a tilt of 0.11 mrad, which corresponds to a displacement of approximately 42 μm at 40 cm from the scattering surface. In order to achieve large displacements, the phase has to wrap many times across the SLM, as can be seen from Fig. 3(a), until the limited spatial resolution can no longer correctly represent the linear gradient. We check the full memory-effect range by physically tilting the SLM and find that it is possible to achieve a displacement of $\pm 1.5^\circ$ losing only 50% of the spot intensity, corresponding to a shift of ± 1 cm at a 40-cm distance from the wall. This indicates that our method can be used to focus light on one side of the barrier and then scan it at the other side by a properly applied phase gradient.

III. RESULTS

After optimizing the focused spot, we replace the camera with an object [see Fig. 4(a)] and perform a 100×100 point scan with a 2.34 mrad (93 μm at 40 cm) step by adding corresponding phase gradients to the SLM pattern

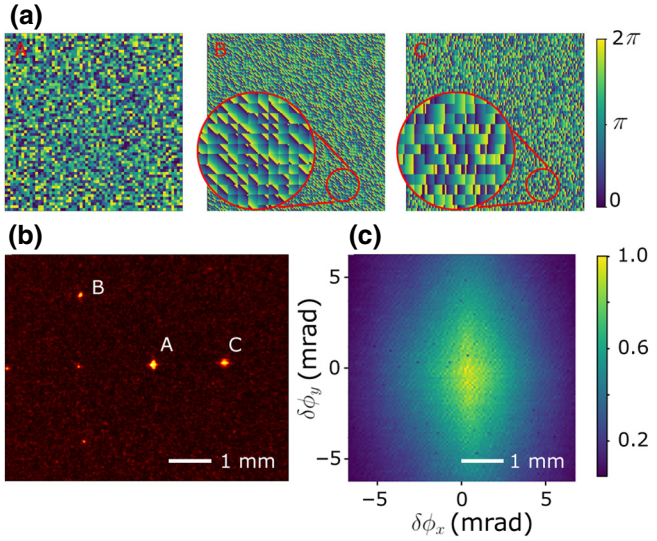

FIG. 3. Manipulating the scattered light: (a) phase patterns on the SLM that correspond to the focused spots A, B, and C in the reflected speckle pattern shown in (b). Additional unlabeled bright spots are artifacts from the diffraction on the macropixels. (c) The attenuation of the focused spot relative to zero displacement. The scale bar refers to 40-cm distance from the wall.

as discussed above. In each of the focus positions, we measure the TOF histogram. Two example TOF histograms of the light collected at the scattering surface are shown in Fig. 4(b): the red solid line is the histogram recorded while the focused spot is hitting the object and the black dashed line shows the background obtained by putting a flat phase pattern on the SLM and thus eliminating the focus. The difference between these two graphs contains information about the object reflectance and, more importantly, allows us to identify the TOF peak (at 2.2 ns) that corresponds to reflection from the object, as it is the one showing the highest variation between the two measurements. We then integrate the temporal histogram data only in a small (0.5 ns) window around this peak. This procedure provides a very effective temporal filter and rejection of background counts, increasing the sensitivity of our method.

The scans of objects A and B obtained by this approach are presented in Fig. 4(c). In these experiments, we use laser power of only around 100 mW, which leads to a return signal from the object of around 6500 counts/s. Such a variation corresponds to only 1.5% of the total detected light intensity, which would make it difficult to reconstruct the object using any of the speckle-memory-effect based methods [7,8]. On the other hand, conventional TOF-imaging techniques would also fail in this scenario, as these rely on detecting the difference in the time of arrival of photons emitted from different points on the object. In our geometry (object at 40 cm from the wall), the maximal difference in the distance to the detector for two points

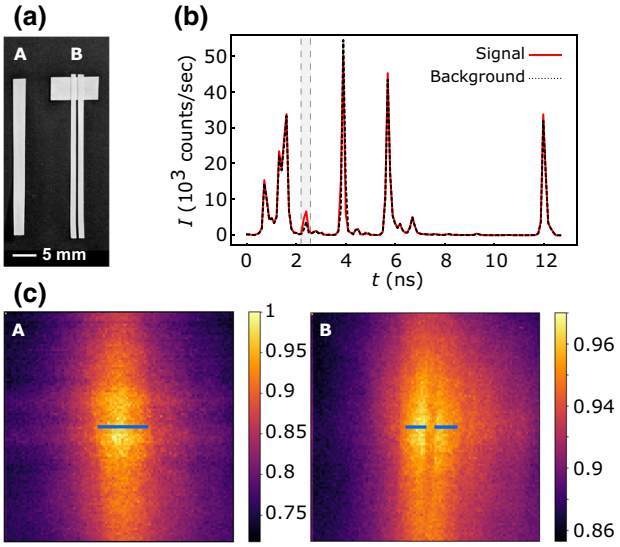

FIG. 4. (a) Two objects that we image with our method. (b) TOF histograms measured with the SPAD: red solid line, the focused spot impinges on the object; black dashed line, without any refocusing (flat pattern on the SLM). The shaded area shows the temporal (TOF) delay corresponding to the object position. (c) Measured images of objects A and B in (a). Blue lines show the actual size of the objects (2.1 mm, object A; 2.8 mm, object B).

separated by 100 μm is approximately 70 μm, which corresponds to a time delay of 0.23 ps, which is far beyond the resolution of any existing time-resolving detector. The resulting images, however, have less contrast toward the edges. Effectively, the reconstructed image is a product of the object's actual shape and the dependence of the focused spot intensity on the displacement angle [Fig. 3(c)].

IV. CONCLUSIONS

We demonstrate an imaging technique based on the combination of TOF reconstruction and speckle-memory-effect-based imaging. Our technique implies focusing light reflected from a rough surface into a single spot by shaping the incident wave front, which then can be displaced using the memory effect. Imaging is achieved by scanning the spot within a particular area and recording TOF histograms of the returned light. The resolution of our method is defined by the size of the focused spot, which can potentially be minimized to the diffraction limit, with the only limitation being the decrease of the total energy within the focus. The time-resolved measurement allows us to detect small changes in the total output signal due to the presence of the object. This allows us to image reflective targets illuminated with the laser placed on the same side of the occluding obstacle as the detector. In addition, this provides information about the object's depth that is not available in the memory-effect-based reconstruction methods, which potentially leads to three-dimensional shape reconstruction. As with any other NLOS method, our technique only works with sparse (small and highly contrasted compared to the background) objects. As it is hard to capture a contribution from such an object in the scattered light, in our current work we have to use a scattering surface with a certain degree of directionality of the scattered intensity. Both of these problems can be solved by improving the focused-spot enhancement. In our work, we can achieve an enhancement factor of approximately 500; however, enhancements of over 10^5 have previously been reported [25]. Such an enhancement would allow us to use our technique with any type of scattering surface and to image less sparse objects. We note, however, that the capture of dark features on a broad-area reflecting surface would still remain a challenge, while the area and resolution of the available SLMs allow us to control only a small fraction of the incident light.

Although, in our current work, we use a camera in place of the object to measure the scattering matrix and focus the reflected light prior to the object reconstruction, the memory effect gives us knowledge about the part of the scattering matrix that we do not measure. We show that its range can be enough for fully noninvasive reconstruction, which can be achieved by focusing on one side of the obstacle and successively displacing the spot behind it. In the current experiment, we cannot achieve that because the SLM is unable to apply a steep linear gradient accurately. This limitation could be eliminated by using, for example, a galvanometric mirror in combination with the SLM. Alternatively, some of the other methods such as the guidestar [26] or nonlinear feedback [27,28] could be used to achieve noninvasive focusing.

ACKNOWLEDGMENTS

This work was supported by the Engineering and Physical Sciences Research Council of the United Kingdom (UK) (EPSRC) under Grants No. EP/M01326X/1 and No. EP/S026444/1, the UK Ministry of Defence (MOD) University Defence Research Collaboration (UDRC) in Signal Processing, and the UK MOD Future Sensing and Situational Awareness Programme.

[1] D. Faccio and A. Velten, A trillion frames per second: The techniques and applications of light-in-flight photography, Rep. Prog. Phys. **81**, 105901 (2018).
[2] I. Freund, Looking through walls and around corners, Physica A **168**, 49 (1990).
[3] A. Kirmani, T. Hutchison, J. Davis, and R. Raskar, in *2009 IEEE 12th International Conference on Computer Vision* (IEEE, Kyoto, 2009), p. 159–166.
[4] N. Naik, C. Barsi, A. Velten, and R. Raskar, Estimating wide-angle, spatially varying reflectance using time-resolved inversion of backscattered light, J. Opt. Soc. Am. A **31**, 957 (2014).

[5] A. Velten, T. Willwacher, O. Gupta, A. Veeraraghavan, M. G. Bawendi, and R. Raskar, Recovering three-dimensional shape around a corner using ultrafast time-of-flight imaging, Nat. Commun. **3**, 745 (2012).

[6] M. O'Toole, D. B. Lindell, and G. Wetzstein, Confocal non-line-of-sight imaging based on the light-cone transform, Nature **555**, 338 (2018).

[7] J. Bertolotti, E. G. Van Putten, C. Blum, A. Lagendijk, W. L. Vos, and A. P. Mosk, Non-invasive imaging through opaque scattering layers, Nature **491**, 232 (2012).

[8] O. Katz, E. Small, and Y. Silberberg, Looking around corners and through thin turbid layers in real time with scattered incoherent light, Nat. Photonics **6**, 549 (2012).

[9] O. Katz, P. Heidmann, M. Fink, and S. Gigan, Non-invasive single-shot imaging through scattering layers and around corners via speckle correlations, Nat. Photonics **8**, 784 (2014).

[10] G. Gariepy, F. Tonolini, R. Henderson, J. Leach, and D. Faccio, Detection and tracking of moving objects hidden from view, Nat. Photonics **10**, 23 (2016).

[11] M. Sanzaro, P. Gattari, F. Villa, A. Tosi, G. Croce, and F. Zappa, Single-photon avalanche diodes in a 0.16 μm bcd technology with sharp timing response and red-enhanced sensitivity, IEEE J. Sel. Top. Quantum Electron. **24**, 1 (2017).

[12] I. M. Vellekoop and A. P. Mosk, Focusing coherent light through opaque strongly scattering media, Opt. Lett. **32**, 2309 (2007).

[13] I. Freund, M. Rosenbluh, and S. Feng, Memory Effects in Propagation of Optical Waves Through Disordered Media, Phys. Rev. Lett. **61**, 2328 (1988).

[14] S. Feng, C. Kane, P. A. Lee, and A. Douglas Stone, Correlations and Fluctuations of Coherent Wave Transmission Through Disordered Media, Phys. Rev. Lett. **61**, 834 (1988).

[15] J. W. Goodman, *Speckle Phenomena in Optics: Theory and Applications* (Roberts & Company, Englewood, 2007).

[16] F. G. Bass and I. M. Fuks, *Wave Scattering from Statistically Rough Surfaces* (Pergamon Press, Oxford, New York, 1979).

[17] I. M. Vellekoop, Feedback-based wavefront shaping, Opt. Express **23**, 12189 (2015).

[18] I. M. Vellekoop and A. P. Mosk, Phase control algorithms for focusing light through turbid media, Opt. Commun. **281**, 3071 (2008).

[19] D. B. Conkey, A. N. Brown, A. M. Caravaca-Aguirre, and R. Piestun, Genetic algorithm optimization for focusing through turbid media in noisy environments, Opt. Express **20**, 4840 (2012).

[20] L. Fang, H. Zuo, Z. Yang, X. Zhang, and L. Pang, Focusing light through random scattering media by simulated annealing algorithm, J. Appl. Phys. **124**, 083104 (2018).

[21] C. W. J. Beenakker, Random-matrix theory of quantum transport, Rev. Mod. Phys. **69**, 731 (1997).

[22] S. M. Popoff, G. Lerosey, M. Fink, A. C. Boccara, and S. Gigan, Controlling light through optical disordered media: Transmission matrix approach, New J. Phys. **13**, 123021 (2011).

[23] A. Albertazzi, M. R. Viotti, F. Silva, C. L. Veiga, E. S. Barrera, M. Benedet, A. V. Fantin, and D. P. Willemann, Speckle Interferometry in harsh environments: design considerations and successful examples, in *Optical Micro- and Nanometrology VII* (International Society for Optics and Photonics, Strasbourg, 2018), Vol. 10678, p. 1067802.

[24] S. M. Popoff, G. Lerosey, R. Carminati, M. Fink, A. C. Boccara, and S. Gigan, Measuring the Transmission Matrix in Optics: An Approach to the Study and Control of Light Propagation in Disordered Media, Phys. Rev. Lett. **104**, 100601 (2010).

[25] H. Yu, K. Lee, and Y. Park, Ultrahigh enhancement of light focusing through disordered media controlled by mega-pixel modes, Opt. Express **25**, 8036 (2017).

[26] R. Horstmeyer, H. Ruan, and C. Yang, Guidestar-assisted wavefront-shaping methods for focusing light into biological tissue, Nat. Photonics **9**, 563 (2015).

[27] O. Katz, E. Small, Y. Guan, and Y. Silberberg, Noninvasive nonlinear focusing and imaging through strongly scattering turbid layers, Optica **1**, 170 (2014).

[28] G. Osnabrugge, L. V. Amitonova, and I. M. Vellekoop, Blind focusing through strongly scattering media using wavefront shaping with nonlinear feedback, Opt. Express **27**, 11673 (2019).